PCIM Europe 2022; International Exhibition and Conference for Power Electronics, Intelligent Motion, Renewable Energy and Energy Management; Proceedings of

Design Optimization of a MW-level Medium Frequency Transformer

N. Djekanovic and D. Dujic

POWER ELECTRONICS LABORATORY
ÉCOLE POLYTECHNIQUE FÉDÉRALE DE LAUSANNE

 DOI:10.30420/565822101

pcim EUROPE

Design Optimization of a MW-level Medium Frequency Transformer

Nikolina Djekanovic, Drazen Dujic

École Polytechnique Fédérale de Lausanne (EPFL), Power Electronics Laboratory, Switzerland

Corresponding author: Nikolina Djekanovic, nikolina.djekanovic@epfl.ch

Abstract

Nowadays, with the increased interest in applications dealing with high-power medium-voltage conversion, there is a strong need to master the design of medium-frequency transformers, which are one of the key components of modern DC transformers. The paper presents the design and development of a 1 MW, 5 kHz core-type transformer prototype, which combines oil-immersed windings, realized as hollow copper conductors with internal deionized water cooling, and nanocrystalline magnetic core material. The design is achieved with the help of a model-based optimization tool, built around elaborate analysis and modeling of medium-frequency transformer specific phenomenon concerning its electrical operation. Moreover, the paper discusses some technical challenges connected to the prototype realization.

1 Introduction

There are several applications where medium voltage direct current (MVDC) grids challenge the existing alternating current systems by providing new and promising solutions. These applications include integration of renewable energy resources, such as off-shore wind energy systems [1], marine all-electric ships [2], and the ever growing big data centers [3]. However, the lack of standardization in the MVDC domain and of suitable protection technologies are among the main reasons for stagnation of practical MVDC grid realizations, thus creating the need for continued research effort. Furthermore, the DC transformer (DCT) is regarded as the key enabling component for future MVDC power distribution networks. Such a device unifies power conversion, insulation and protection into a single power electronics system. The DCT is based on resonant energy conversion combined with high-voltage switching devices, providing bidirectional power flow in open-loop operation, which reduces the overall control effort [4]. Additionally, resonant converter topologies are being increasingly employed, mostly due to their soft switching capabilities, which provide increased efficiency [5].

The voltage adaptation and galvanic insulation are provided by the medium frequency transformer (MFT). In general, the design of magnetic components today is mainly computer-aided and performed with the help of design optimization tools, which are structured to include all the relevant component aspects through corresponding models. These address insulation and thermal coordination, core and winding losses, estimation of leakage and magnetizing inductance and so on. To decrease the computational weight and execution time, the models used in the design tool need to be simple and fast to execute, yet sufficiently precise and accurate. In the recent literature a significant effort was made in the direction of mastering the design optimization of MFTs [6]–[8]. Thereby, various combinations of technologies, regarding cooling and insulation, magnetic materials and conductor types were analyzed and modeled, resulting in new and improved models and MFT prototypes. Moreover, the optimizations methods themselves were studied, which led to the use of more advanced genetic algorithms and artificial intelligence, i.e. neural networks, to achieve better results faster [9].

Yet, vast majority of the realized prototypes is downscaled and in the range of several tens of kilowatts endorsing the modular way of power processing [6]–[8]. Nevertheless, bulk power conversion offers easier overall integration of a power electronic system, due to the lower number of components which establishes higher reliability and facilitates system optimization and design. On that account,

ISBN 978-3-8007-5822-7

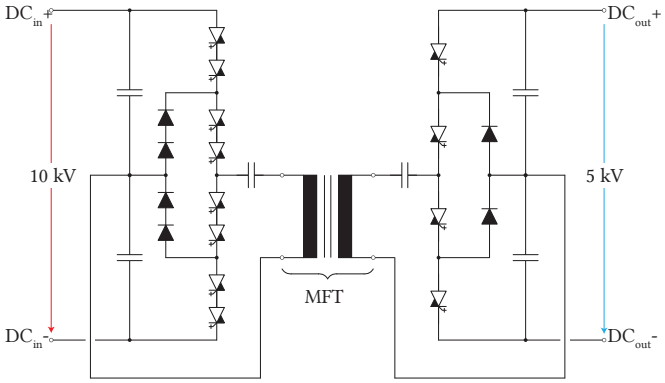

Fig. 1: DCT design concept based on the LLC resonant converter.

this paper presents a 1 MW MFT prototype, including the complete design optimization process and experimental verification.

The MFT is envisioned as an integral part of a series resonant DC-DC converter, which uses integrated gate-commutated thyristors (IGCTs) as switching devices, due to their high current conducting capabilities and low conduction losses [10]. Owing to processing of high powers, the semiconductor devices are cooled with deionized (DI) water, which is selected as the cooling solution for the MFT as well. The two power stages, interconnected with the transformer and the resonant capacitors, are based on the 3-level neutral point clamped (NPC) topology, with split-capacitors used as the second leg, presented in Fig. 1. In order to reach higher MVDC voltages, the primary side requires a series connection of 4.5 kV IGCTs [11] and it is supplied by a 10 kV DC-link, whereas the secondary side operates with a 5 kV DC-link. Therefore, the rated primary and secondary voltages of the MFT under analysis are ± 5 kV and ± 2.5 kV, respectively. In the case of the selected LLC resonant topology, the MFT is intrinsically part of the resonant tank with its leakage and magnetizing inductance, which stresses the need for accurate modeling and design of this aspect. At last, the electrical requirements, derived from the DCT design specifications and governing the transformer design, are summarized in Tab. 1. For flexibility reasons, a target range is defined for both magnetizing and leakage inductance. The reference range of the former parameter corresponds to the turn-off (magnetizing) current of roughly 6 A$-$10 A at the primary side.

In summary, this paper presents a core-type transformer with hollow copper conductors as windings,

Tab. 1: MFT electrical requirements.

Characteristics	Unit	Value
Frequency	kHz	5
Nominal power	MW	1
Turns ratio	1	2 : 1
Primary voltage	kV	± 5
Secondary voltage	kV	± 2.5
Ref. magn. inductance	mH	$25 - 40$
Ref. leakage inductance	µH	$25 - 50$

suitable for internal DI water cooling, which are additionally oil-immersed for insulation purposes. The developed design tool optimizes the combination of selected technologies in order to achieve the best performing MFT design.

2 MFT Design Optimization

Reaching an optimal MFT design for a certain set of electrical requirements implies without exception solving a complex nonlinear multi-objective problem. The designers are interested in knowing the performance limits, i.e. the highest feasible efficiency, yet with the lowest attainable gravimetric and volumetric power densities. The final selection of the optimal design is eventually a compromise between multiple, often opposing, design characteristics. Furthermore, design optimization of commercial MFTs considers the overall production cost as another important design criterion.

The design optimization algorithm presented in this paper is based on the well-known and reliable brute-force concept and it is devised to design three variations of core-type transformers, namely: 1) 1-layer MFT (one layer of the primary winding (PW) and one layer of the secondary winding (SW) in a single oil vessel placed around one of the two core limbs); 2) 2-vessel MFT (two oil vessels, placed around each of the core limbs, each containing one layer of PW and one layer of SW) and 3) 3-winding MFT structure (PW is interleaved and placed concentrically around the SW in a single oil vessel). General design concepts of the three options are illustrated in Fig. 2. Considering the desired turns ratio of 2:1, the first MFT option implies different cross section profiles should be used for the windings, if the goal is to optimally use the space inside of the oil vessel, i.e. to achieve similar heights of both windings. As

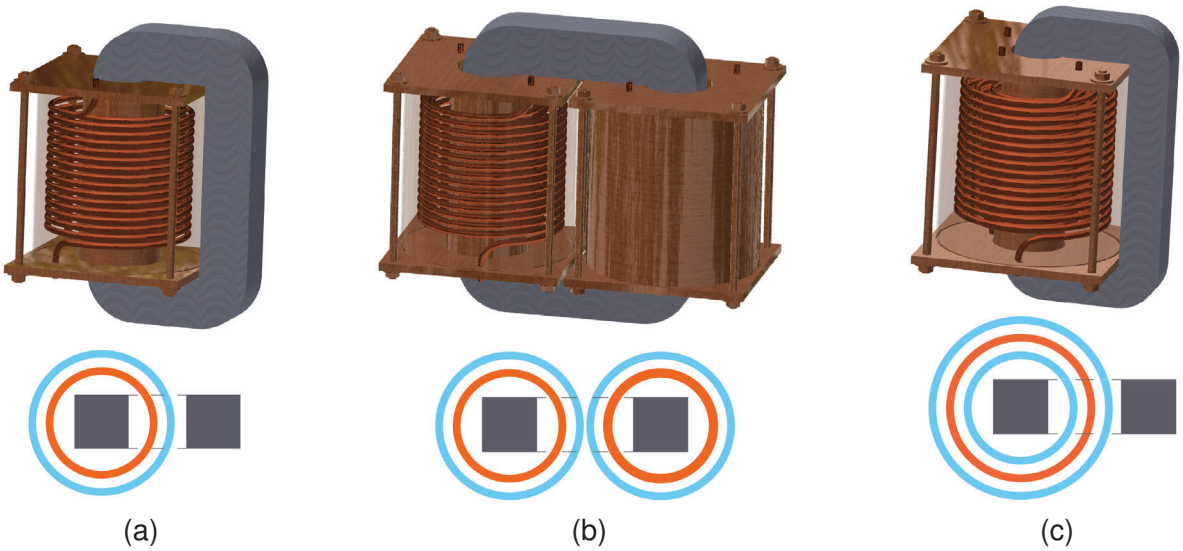

Fig. 2: General design concept of (a) 1-layer, (b) 2-vessel and (c) 3-winding MFT structure with corresponding top cross section views. PWs are illustrated with blue and the SWs with orange color.

a result, this imposes additional challenges on the practical realization and disrupts axial symmetries. As for the 2-vessel MFT, having the PWs connected in series and the SWs in parallel allows the use of the same conductor type and enforces equal current densities in all the windings, which restores transformer symmetries and simplifies modeling. The 3-winding MFT structure proved to be interesting for similar reasons as the 2-vessel type, with additionally improved power densities. However, having the same conductor type for both windings implies SW current density is two times bigger than the PW one.

To allow internal water cooling, the transformer windings are designed in the form of round copper hollow conductors. Nevertheless, there are manufacturing and mechanical constraints on the conductor's cross section profile, which include limited wall thickness, but also a required bending radius for the winding termination, both depending on the external diameter of the cross section. Moreover, considering the copper skin depth at the set operating frequency (below 1 mm at 5 kHz) implies the presence of the skin effect and it is a disadvantage that needs to be reckoned with.

Having additionally oil-immersed windings has a positive effect on the overall MFT power density, due to reduced required insulation distances compared to air isolation. For this purpose, biodegradable synthetic ester transformer fluid Midel 7131 is selected [12], which provides superior dielectric and thermal properties (increased fire safety, high dielectric breakdown above 75 kV according to IEC 61099 [13]) compared to standard mineral oils used for transformer insulation. The core itself is air-cooled and not in contact with oil. For an optimal design, the algorithm is able to consider various magnetic core materials, namely, grain oriented electrical steel, amorphous and nanocrystalline material.

Fig. 3 provides an overview of the implemented design optimization algorithm, which is an extension of work conducted in [7]. The blue boxes stand for the user-defined input blocks, such as electrical requirements, various constraints regarding insulation, thermal and mechanical considerations, as well as available data sheets and material characteristics. The orange designates the design space forming step, where each combination of optimization variables describes a specific MFT design. In the considered algorithm, the design variables are the internal hollow conductor diameter (D_i) and the corresponding wall thickness (δ), which is defined as multiple of the frequency-dependent skin depth, the SW turns number (N_{SW}) and the ratio between the set flux density amplitude and the saturation density of the magnetic material (K_{bm}). Tab. 2 specifies the upper and lower boundary of each of the design variables, together with the number of resolution points. Furthermore, the green-colored boxes represent the design evaluation part of the optimization process, consisting of various relevant

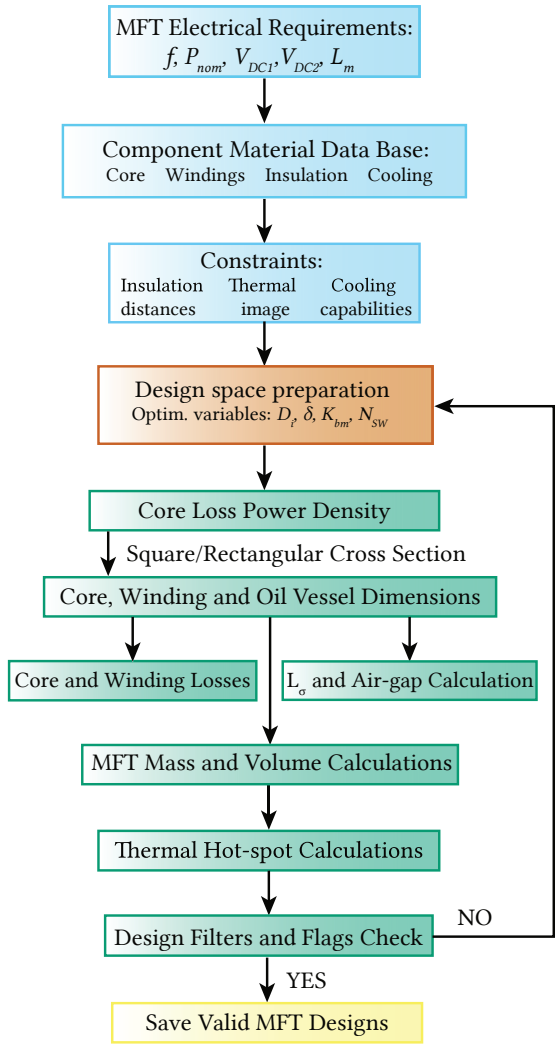

Fig. 3: Design optimization algorithm flowchart. Blue: user-defined inputs; Orange: design space forming; Green: optimization process; Yellow: valid MFT designs.

MFT models. Eventually, each design that passes all the user-defined design filters and constraint flags check is marked as a valid MFT design. In the final step highlighted with yellow these designs are saved into a database.

Considering the employed models, the core loss calculation is based on the Improved generalized Steinmetz equation from [14], which is able to provide accurate estimations for non-sinusoidal voltage excitations. In case of large core cross-section areas, the algorithm can take into account production limits of specific core materials and branch out to designs with rectangular cross sections. This is the second option besides the default square core cross section option, which optimally uses the area of the inner hollow cylinder of the oil vessel.

Tab. 2: Design optimization variables.

Var.	Min.	Max.	Res.	Description
D_i	3 mm	8 mm	16	Inner diameter
δ	$0.9\delta_{Cu}$	$2.2\delta_{Cu}$	14	Wall thickness
N_{SW}	10	45	36	SW turns No.
K_{bm}	0.2	0.9	80	Flux dens. ratio

For modeling of hollow conductor winding losses a FEM-obtained factor, which characterizes the frequency-dependent AC resistance of hollow conductors in particular, is used in combination with the well-known Dowell's model [15]. The adequate magnetizing inductance is determined by the turn-off current of the switching devices and affects in turn the core air gap. Furthermore, the analytical model of the leakage inductance is based on the Margueron's model [16]. Nevertheless, at this point the eddy current effect that decreases the leakage inductance value at elevated frequencies is observed only with FEM simulations.

Due to specificity of the selected technologies, i.e. forced water cooling and natural-convection based insulation, an analytical thermal-hydraulic model (THM), which describes the thermal behavior of the insulation oil, is developed along with the static thermal model to aid the estimation of the overall transformer thermal image. The THM, developed by the authors, is able to accurately estimate characteristic oil temperatures, depending on the winding losses and the cooling conditions. The model implementation is based on analytical equations, describing the thermal and the hydraulic sides of oil circulation caused by natural convection, combined with experimental thermal measurements and multi-objective optimization. Natural oil circulation is achieved by the fact that DI water of lower temperature, compared to the average conductor temperature, enters the windings at the top and leaves heated at the bottom, which causes a temperature gradient to form along the windings. Increased temperature of the windings at the bottom warms the surrounding oil, which contributes to a decrease in density and oil expansion, i.e. buoyancy forces drive the oil towards the top. Since the windings are colder at the top, the oil will decrease its temperature, become heavier (increased density) and come down to the bottom. At the same time, there is a heat exchange between the oil and the vessel, which additionally reduces the oil temperature. Fig. 4

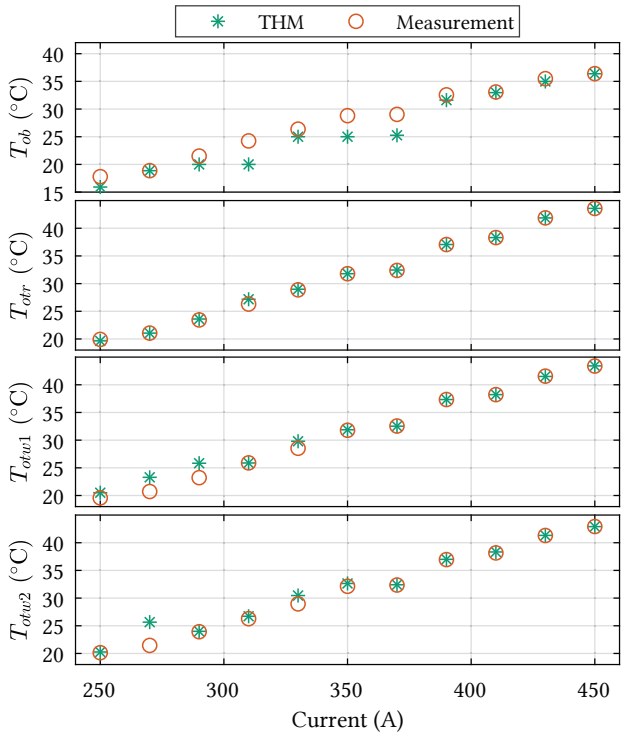

Fig. 4: Experimentally obtained oil temperatures versus THM output results at various operating points (250 A – 450 A DC range corresponds to roughly 1 kW – 3 kW total winding losses.)

shows the comparison between the measured oil temperatures and the estimated ones for various winding losses, which are induced by a controlled DC power supply. Detailed description of the model and the experimental setup can be found in [17]. Note that thermal modeling of the MFT is not the topic of the paper at hand and it will not be discussed further. As one of the novel design filters, the algorithm offers the possibility of influencing the core to winding loss ratio (R_{wc}) during the design phase. In this way, due to availability of aggressive DI water cooling, the majority of the losses can be forced to the windings.

To reduce design complexity, many parameters are set to constant values, such as wall and lid thickness of the oil vessels. The two values, along with the vessel material, are determined together with the manufacturer (Elektro-Isola [18]), considering the weight of the contained oil and windings and the highest temperatures that can be reached. The insulation distance between the PW and SW, and between the surrounding vessel walls and each of the windings are set to constant values, according to the dielectric properties of the insulation fluid. A practical constraint to have in mind is the minimal

Tab. 3: Constant parameters.

Par.	Value	Description
v_d	3 mm	Turn-to-turn distance
$d_{PW,SW}$	8 mm	PW-to-SW distance
d_{hor}	10 mm	Winding to vert. wall dist.
d_{ver}	20 mm	Winding to lid distance
T_{in}	30 °C	Inlet coolant temperature
Q_{fl}	10 L min^{-1}	Coolant volumetric flow

distance necessary for the oil to reach all the areas, and thus avoid forming of air bubbles inside of the vessels. Additionally, the inlet temperature and the volumetric flow of the coolant are set according to the worst cooling conditions, in order to rule out the designs which do not comply with thermal constraints and to have robust MFT designs. The worst conditions imply reaching the pressure drop limit of the DI water cooling unit (achieved with high volumetric flow, long windings and small conductor's inner diameter) and having maximal available inlet coolant temperature. The constant parameters are summarized in Tab. 3.

Finally, for the particular design of the MFT presented in this paper, the main design criterion is to achieve maximal efficiency. Consequently, this comes at the cost of increased weight and volume, i.e. low gravimetric and volumetric power densities. To clarify, the high efficiency requirement corresponds to the fact that the discussed MFT is intended for use in the MVDC distribution networks, where the necessary weight or space are usually not inhibited in any way.

3 1MW MFT Prototype

Initially conducted studies show that of the three considered transformer types, the 2-vessel MFT in combination with nanocrystalline magnetic material yields the highest operating efficiency ($\eta = 99.18\%$). Yet, the 3-winding MFT with the same core material follows closely the performance ($\eta = 99.02\%$) of the selected option. Note that the specified efficiencies give theoretical values, i.e. design tool outputs, and are not electrically measured at this point. As already mentioned, to achieve the turns ratio requirement of $2:1$, the PWs from the two vessels need to be connected in series, and the SWs in parallel. However, this represents only one of the possible configurations, considering that the selected MFT

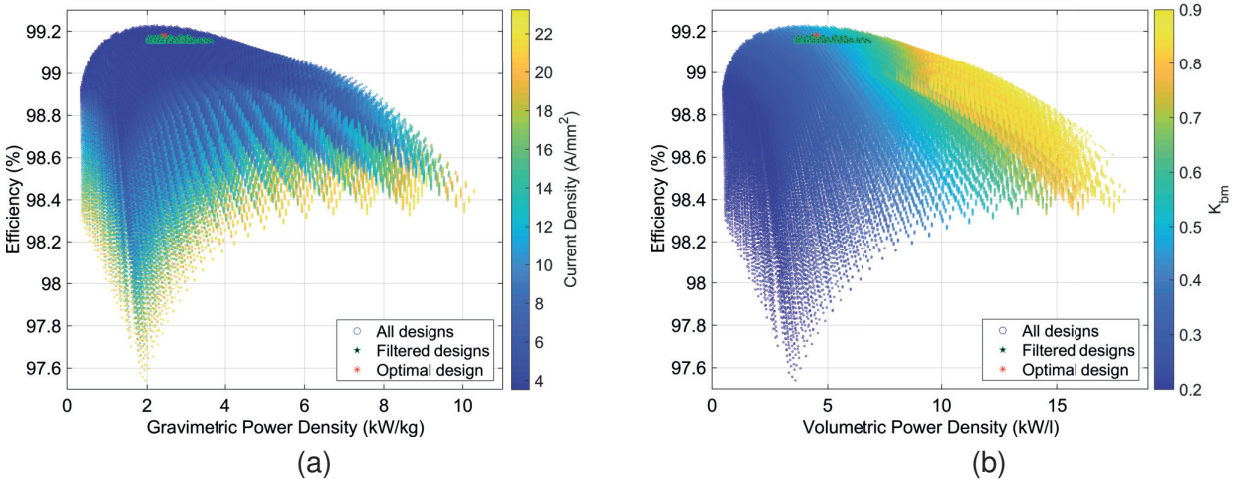

Fig. 5: Plots of generated MFT designs with nanocrystalline material at 5 kHz: (a) Efficiency vs. weight power density; (b) Efficiency vs. volume power density. Minimal efficiency of the filtered designs is 99.15 %.

type has four separate windings. The appendix provides details of the other configurations and their corresponding electrical connections, making the prototype extremely versatile for various research.

Fig. 5 shows efficiency plots with all the MFT designs obtained from the optimization tool, by varying the selected design variables according to their respective ranges from Tab. 2. Thereby, the color code of each plot can be set to any of the MFT parameters to help designers observe the existing trends. For example, high values of current density in Fig. 5a corresponds to reduced cross-section area of the conductor which leads to increased winding losses and reduced efficiency. On the other hand, higher K_{bm} factor, observed in Fig. 5b, positively affects the mass and volume of the MFT, since for higher flux densities, the core cross section reduces, but it causes an increase in the core losses, which influences the efficiency. The upper boundary lines of the two feasibility plots are known as the Pareto front, which represents a trade-off between maximum achievable efficiency and power density. Its descending trend shows that efficiency must be sacrificed for an increase in power density. The lower boundary lines provide information about the thermal limits. According to Fig. 5, an increase in power density of a design at the thermal limit, which implies size reduction that in turn compromises cooling conditions, is thermally feasible only if the losses are reduced, that is for increased efficiency. The filtered designs marked with green stars represent valid MFT designs which in addition comply with current densities above 6 A mm^{-2}, the core to winding loss ratio below 33%, a minimal power density of 2 kW kg^{-1} and a minimal efficiency of 99.15%. Eventually, the optimal design from this prefiltered group is selected based on the highest achievable efficiency and its specifications are given in Tab. 4. The 3D rendered model of the MFT with additional parts intended for support and fixation is shown in Fig. 6 (the termination panel is not shown). The top and bottom aluminum plates act as a vertical clamp, providing stability to the structure. The lower white plastic E-shaped supports help distribute the weight of the vessels and together with the upper supports compress and keep the vessel structure in place.

Tab. 4: Selected optimal 2-vessel MFT design specifications corresponding to the highest efficiency design.

D_i	δ	N_{PW}	N_{SW}	K_{bm}	$P_{loss,PW}$	$P_{loss,SW}$	P_{core}
7.6 mm	1.3 mm	34	17	0.475	2.87 kW	2.67 kW	2.67 kW
R_{wc}	J	kW/kg	kW/l	W	L	H	η
0.32	6.1 A mm^{-2}	2.36	3.47	494 mm	851 mm	685 mm	99.18%

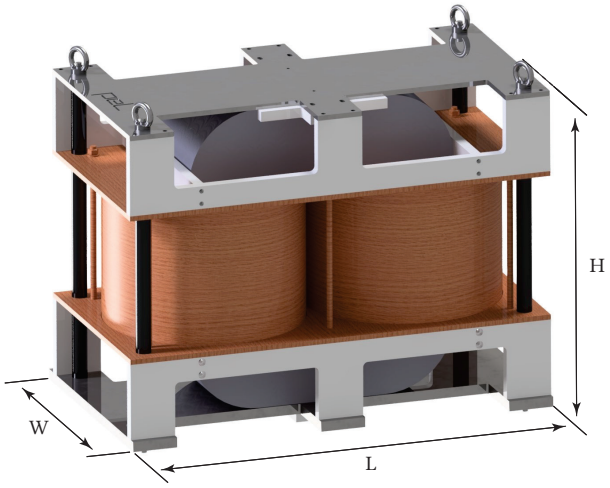

Fig. 6: 3D CAD render of the 2-vessel core type MFT.

As previously mentioned, the transformer windings are realized in the form of hollow pipes, made of soft temper copper for easier manipulation and produced by Luvata [19]. Nevertheless, bending of copper pipes to obtain two PW and SW sets of 17 turns each, with fixed external winding diameters and a fixed turn-to-turn distance, proved not to be an easy task. In order to ensure the required distances and add stability, six comb-alike spacers are added per winding, made of thermoplastic material POM, which can be seen in Fig. 7. On top of that, the spacers provide the required distance between the windings and the vessel walls. Another peculiarity of the windings is the fact that both PWs are wound regarding the right chirality, that is in the mathematical or the counterclockwise direction, whereas the SWs are wound conversely, according to the left chirality.

Moreover, to ensure that the insulation fluid will not leak out of the vessel at the winding-vessel lid

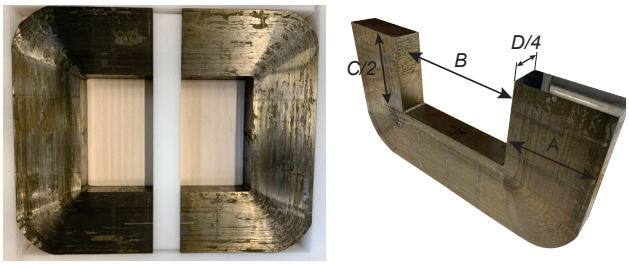

(a) (b)

Fig. 8: MFT magnetic core made of nanocrystalline: (a) Set of two C-cut cores; (b) Single C-cut core.

contact, seal connectors with rubber washers are brazed at the top and bottom of each winding. In addition, the bottom vessel lid is glued to the cylinder walls, whereas the top part can be removed. Regarding insulation, the fluid is poured to a predetermined level (until the windings are fully covered), leaving an air pocket in each vessel, which provides space for the oil to expand during transformer operation. The displaced air leaves the vessel through an air breather filled with silica gel, which acts as drying agent and keeps moisture away from the insulation fluid.

Due to manufacturing limits, the transformer core is assembled from four sets (two C-cut cores per set), made of nanocrystalline Finemet material (52 mm wide tapes) and produced by Hitachi Metals [20], as shown in Fig. 8. Eventually, due to the same reason, the core cross-section area is of rectangular shape. The dimensions of the assembled core are provided in Tab. 5, along with its weight. The two C-cut cores are held in set with a help of a custom-tailored stainless steel band. The fully assembled core is held in place by supporting structures in the other two remaining dimensions. Owing to the specific way the core sets are held together and to reach the

(a) (b) (c)

Fig. 7: MFT oil vessels, made of phenolic paper composite material Etronit I and B66, each containing a set of PW and SW with spacers and the insulation liquid: (a) Left vessel; (b) In between the vessels; (c) Right vessel.

ISBN 978-3-8007-5822-7

Tab. 5: Properties of the fully assembled MFT core.

A	B	C	D	M_c
140 mm	256 mm	318 mm	232 mm	≈ 401 kg

required magnetizing inductance, the air gap has to be adjusted separately for each set. Finally, the assembled 1 MW MFT prototype is shown in Fig. 9.

4 MFT Electrical Parameters

The first conducted measurements with the MFT prototype deal with verification of its required electrical parameters, namely, the leakage and magnetizing inductance. For this purpose, two measurement devices are employed, an RLC meter (BK895), which measures impedances at fixed predefined frequencies, and the Omicron Lab Bode 100, which works as impedance analyzer for a certain frequency range. Depending on the winding side where the measurements are performed, different values can be expected. Note that the requirements made in Tab. 1 are referred to the primary side. All the measurements are subsequently compensated for the inductances of the short-circuit cables, as well as the connecting cables of the used measuring instruments.

The measured leakage inductance values at the primary side are compared with the analytical

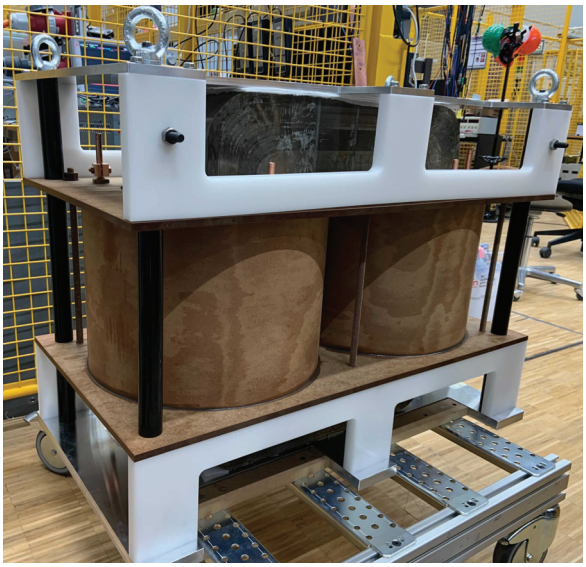

Fig. 9: Full-scale prototype of 2-vessel core type MFT. The termination panel and the DI water distribution pipes are not shown.

Tab. 6: Comparison of measured and modeled characteristic MFT inductances.

L_σ(µH)	An.model	FEM	RLC	Bode 100
0 Hz	43.8	44.3	–	–
5 kHz	–	34	38.2	37.9

L_m(mH)	Ref. value	RLC	Bode 100
5 kHz	35.77	36.66	36.74

model used in the optimization tool, and with FEM-simulated values, as given in Tab. 6. The analytical model is based on the method of magnetic images and it is frequency-independent. On the other hand, the RLC meter is able to measure impedances down to 20 Hz, for the Bode 100 the value is 100 Hz. As for FEM simulations conducted in Comsol, both windings are modeled as perfect helixes in 3D, together with the core. However, to reduce the computational time and burden, the leakage inductance calculations are performed in 2D, obtained from a vertical cross section of the 3D model. These simplifications explain the slight deviations from the measured values. Nevertheless, an overall agreement between the modeled and simulated values at 0 Hz, and modeled and measured values at the operating frequency prevails. All the values lie in the required range stated in Tab. 1.

While the leakage inductance is predominantly determined by the geometry of the windings, the magnetizing inductance can be controlled by adjusting the air gap between the core sets. Furthermore, its value is determined by the MFT magnetizing current, which is for the selected resonant converter topology also the turn-off current. Regarding the measurements of the magnetizing inductance, the air gap is set to around 1 mm, which, according to analytical calculations, corresponds to the stated reference value and a turn-off current of 7 A. According to Tab. 6, the reference closely matches the measured ones. The final air gap value will be set during the commissioning of the DCT.

5 Conclusion

This paper provides detailed insight into the design and development of a 1 MW, 5 kHz core-type MFT, intended for bulk power processing as a part of a DC transformer. The prototyped design combines various technologies for cooling and insulation (DI

water and biodegradable synthetic ester fluid, particularly for the windings) and nanocrystalline as the magnetic core material. The selected design is a result of design optimization process, applied to a set of predefined electrical MFT requirements. The model-based design tool is presented based on the flowchart of the algorithm behind. In addition, the thermal-hydraulic model of the circulating oil developed by the authors is briefly introduced. To reach the required turns ratio, the PWs are connected in series and the SWs in parallel. However, the assembled MFT prototype is esentially a 4-winding transformer and can be used in numerous other ways with correct external winding connections. All the usable configurations are summarized in the appendix.

Furthermore, several technical difficulties are discussed, such as core manufacturing limits which forced a rectangular core cross section, and mechanical constraints relevant for dealing with hollow copper conductors employed as MFT windings.

The electrical measurements regarding the leakage and magnetizing inductance performed on the prototype fulfill the requirements and show a good agreement between the measured and the estimated values from the design tool.

Acknowledgment

The results presented in this paper are a part of the EMPOWER project that has received funding from the European Research Council (ERC) under the European Union's Horizon 2020 research and innovation programme (Grant agreement No. 818706).

Appendix

Fig. 10 provides a review of all the functional MFT configurations. Depending on the external connections of the windings and attributions of PWs and SWs in the two vessels, the prototype can be used for eight 2-winding configurations, presented in subfigures (a) and (b) of Fig. 10. Additionally, six 3-winding options are identified, shown in (c), and a single 4-winding MFT option exists, given in (d).

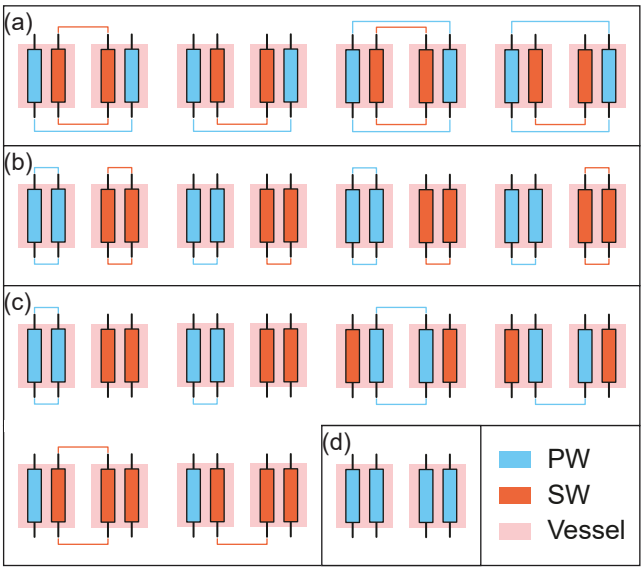

Fig. 10: Usable prototype configurations of 2-winding MFT with: (a) a pair of PW and SW in each vessel; (b) PWs and SWs in separate vessels; (c) 3-winding MFTs; (d) 4-winding MFT.

References

[1] Y.-H. Chen, C. Dincan, R. Olsen, M.-C. Schimmelmann, P. Kjær, and C. Bak, "Studies for characterisation of electrical properties of dc collection system in offshore wind farms," in *Proceedings of CIGRÉ general session 2016*, CIGRE, 2016.

[2] U. Javaid, D. Dujić, and W. van der Merwe, "Mvdc marine electrical distribution: Are we ready?" In *IECON 2015 - 41st Annual Conference of the IEEE Industrial Electronics Society*, 2015, pp. 823–828.

[3] B. R. Shrestha, U. Tamrakar, T. M. Hansen, B. P. Bhattarai, S. James, and R. Tonkoski, "Efficiency and reliability analyses of ac and 380v dc distribution in data centers," *IEEE Access*, vol. 6, Oct. 2018.

[4] J. Kucka and D. Dujic, "Smooth power direction transition of a bidirectional llc resonant converter for dc transformer applications," *IEEE Transactions on Power Electronics*, vol. 36, no. 6, pp. 6265–6275, 2021.

[5] M Salem, A Jusoh, N. R. N. Idris, and I. Alhamrouni, "Performance study of series resonant converter using zero voltage switching," in *2014 IEEE Conference on Energy Conversion (CENCON)*, IEEE, 2014.

[6] A. Bahmani, “Design and optimization considerations of medium-frequency power transformers in high-power dc-dc applications,” Ph.D. dissertation, Chalmers Tekniska Hogskola (Sweden), 2016.

[7] M. Mogorovic, “Modeling and design optimization of medium frequency transformers for medium-voltage high-power converters,” Ph.D. dissertation, EPFL, 2019.

[8] T. Guillod, “Modeling and design of medium-frequency transformers for future medium-voltage power electronics interfaces,” Ph.D. dissertation, ETH Zurich, 2018.

[9] T. Guillod and J. W. Kolar, “From brute force grid search to artificial intelligence: Which algorithms for magnetics optimization?” In *35th IEEE Applied Power Electronics Conference (APEC 2020)*, 2020.

[10] D. Stamenković, U. R. Vemulapati, T. Stiasny, M. Rahimo, and D. Dujić, “IGCT low-current switching— TCAD and experimental characterization,” *IEEE Transactions on Industrial Electronics*, vol. 67, no. 8, pp. 6302–6311, 2019.

[11] G. Ulissi, U. R. Vemulapati, T. Stiasny, and D. Dujic, “High-frequency operation of series-connected igcts for resonant converters,” *IEEE Transactions on Power Electronics*, vol. 37, no. 5, pp. 5664–5674, 2022.

[12] *Midel 7131*, https://www.midel.com/.

[13] IEC61099, *Insulating Liquids-Specifications for Unused Synthetic Organic Esters for Electrical Purposes, Switzerland*, 2010.

[14] K. Venkatachalam, C. R. Sullivan, T. Abdallah, and H. Tacca, “Accurate prediction of ferrite core loss with nonsinusoidal waveforms using only steinmetz parameters,” in *2002 IEEE Workshop on Computers in Power Electronics, 2002. Proceedings.*, IEEE, 2002.

[15] F Lü, Y. Guo, Y. Wang, D. Yu, and P. Li, “Ac resistance calculation method for hollow conductor windings in high power medium frequency transformers,” in *Proceeding of the CSEE*, vol. 36, 2016, pp. 6552–6558.

[16] X. Margueron, A. Besri, P.-O. Jeannin, J.-P. Keradec, and G. Parent, “Complete analytical calculation of static leakage parameters: A step toward hf transformer optimization,” *IEEE Transactions on Industry Applications*, vol. 46, no. 3, pp. 1055–1063, 2010.

[17] N. Djekanovic and D. Dujic, “Modeling and characterisation of natural-convection oil-based insulation for medium frequency transformers,” in *2022 IEEE Applied Power Electronics Conference and Exposition (APEC)*, 2022, Accepted.

[18] *Elektro-Isola A/S, Denmark*, https://www.elektro-isola.com/.

[19] *Luvata Pori Oy, Finland*, https://www.luvata.com/.

[20] *Hitachi Metals Ltd. Japan*, https://www.hitachi-metals.co.jp/e/.